

## [O I] disk emission in the Taurus star-forming region

G. Aresu<sup>1,2</sup>, I. Kamp<sup>1</sup>, R. Meijerink<sup>1,3</sup>, M. Spaans<sup>1</sup>, S. Vicente<sup>1</sup>, L. Podio<sup>5,6</sup>, P. Woitke<sup>4</sup>, F. Menard<sup>5,7</sup>, W.-F. Thi<sup>5</sup>,  
M. Güdel<sup>8</sup>, and A. Liebhart<sup>8</sup>

<sup>1</sup> Kapteyn Astronomical Institute, Postbus 800, 9700 AV Groningen, The Netherlands  
e-mail: giambattista.aresu@gmail.com

<sup>2</sup> INAF, Osservatorio Astronomico di Cagliari, via della Scienza 5, 09047 Selargius, Italy

<sup>3</sup> Leiden Observatory, Leiden University, PO Box, 2300 RA Leiden, The Netherlands

<sup>4</sup> SUPA, School of Physics and Astronomy, University of St. Andrews, St. Andrews KY16 9SS, UK

<sup>5</sup> UJF-Grenoble, CNRS-INSU, Institute de Planétologie et d'Astrophysique (IPAG) UMR 5274, France

<sup>6</sup> INAF – Osservatorio Astrofisico di Arcetri, Largo E. Fermi 5, 50125 Florence, Italy

<sup>7</sup> UMI-FCA (UMI 3386), CNRS/INSU France and Universidad de Chile, 1058 Santiago, Chile

<sup>8</sup> University of Vienna, Department of Astronomy, Türkenschanzstrasse 17, 1180 Vienna, Austria

Received 6 August 2013 / Accepted 11 February 2014

### ABSTRACT

**Context.** The structure of protoplanetary disks is thought to be linked to the temperature and chemistry of their dust and gas. Whether the disk is flat or flaring depends on the amount of radiation that it absorbs at a given radius and on the efficiency with which this is converted into thermal energy. The understanding of these heating and cooling processes is crucial for providing a reliable disk structure for interpreting dust continuum emission and gas line fluxes. Especially in the upper layers of the disk, where gas and dust are thermally decoupled, the infrared line emission is strictly related to the gas heating/cooling processes.

**Aims.** We aim to study the thermal properties of the disk in the oxygen line emission region and to investigate the relative importance of X-ray (1–120 Å) and far-UV radiation (FUV, 912–2070 Å) for the heating balance there.

**Methods.** We use [O I] 63 μm line fluxes observed in a sample of protoplanetary disks of the Taurus/Auriga star-forming region and compare it to the model predictions presented in our previous work. The data were obtained with the PACS instrument on board the *Herschel* Space Observatory as part of the *Herschel* open time key program GAS in Protoplanetary diskS (GASPS).

**Results.** Our theoretical grid of disk models can reproduce the [O I] absolute fluxes and predict a correlation between [O I] and the sum  $L_X + L_{FUV}$ . The data show no correlation between the [O I] line flux and the X-ray luminosity, the FUV luminosity or their sum.

**Conclusions.** The data show that the FUV or X-ray radiation has no notable impact on the region where the [O I] line is formed. This contrasts with what is predicted from our models. Possible explanations are that the disks in Taurus are less flaring than the hydrostatic models predict and/or that other disk structure aspects that were left unchanged in our models are important. Disk models should include flat geometries, varying parameters such as outer radius, dust settling, and the dust-to-gas mass ratio, which might play an equally important role for the [O I] emission. To improve statistics and draw more robust conclusions on the thermal processes that dominate the atmosphere of protoplanetary disks surrounding T Tauri stars, more  $L_{FUV}$  and  $L_X$  measurements are needed. High spatial and spectra resolution data is required to disentangle the fraction of [O I] flux emitted by the disk in outflow sources.

**Key words.** protoplanetary disks

### 1. Introduction

Planet formation is strongly linked to the physical properties of the parent disk. Important constraints on the timescale for the gas accretion of giant planets are posed by photoevaporation models. The results of such models are essential in order to estimate the mass loss rates, hence the survival time of gas in disks (Alexander et al. 2006; Ercolano et al. 2008; Gorti et al. 2009). The stellar radiation, especially in the high energy regime ( $E > 6$  eV), is responsible for the thermo-chemical conditions in the disk atmosphere, since it provides most of the energy that causes the gas temperature to exceed the dust temperature there (Kamp & Dullemond 2004; Jonkheid et al. 2004; Glassgold et al. 2004). However, the thermal processes that heat and shape protoplanetary disks are poorly constrained and can only be indirectly measured through cooling lines. One of the dominant cooling lines that can be used to understand these processes is the 63 micron line of neutral oxygen (Gorti & Hollenbach 2008; Meijerink et al. 2008; Woitke et al. 2009; Aresu et al. 2012).

T Tauri stars emit radiation at high energies, owing both to chromospheric activity and accretion of disk material onto the stellar surface. The far-ultraviolet (FUV) luminosity between 7 and 10 eV ( $\Delta\lambda = 1240\text{--}1770$  Å), has been measured by Yang et al. (2012) for a sample of accreting sources in Taurus: they find values between  $10^{30}$  and few times  $10^{32}$  erg/s. The emission is in excess when compared to the stellar emission in the same energy band for non-accreting young stars of the same spectral type. This suggests that accretion is responsible for this emission, in which case it is caused by shocks created by the magnetic field that channels disk material toward the stellar surface (Calvet & Gullbring 1998; Valenti et al. 2000). EUV ( $\Delta\lambda = 120\text{--}912$  Å,  $\Delta E = 13.6\text{--}100$  eV) radiation is believed to mainly affect the upper disk surface at small radii, since the high cross section for absorption only allows penetration of small columns of  $N_H \sim 10^{19}$  cm<sup>-2</sup>. The XEST survey (Güdel et al. 2007) has shown that young stars are also active X-ray emitters, mainly thanks to chromospheric activity, and can reach luminosities between  $10^{29}$  and  $10^{31}$  erg/s.

The high energy depositions ( $>0.01 L_{\odot}$ ) and heating efficiencies ( $\sim 30\%$ ) of X-rays cause the tenuous disk atmosphere to heat up to temperatures of a few thousand Kelvin (Glassgold et al. 2007; Nomura et al. 2007; Gorti & Hollenbach 2008; Ercolano et al. 2008; Aresu et al. 2011).

Recent observations, carried out with the *Herschel* Space Observatory toward the Taurus star-forming region, offer the chance to test model predictions on the thermal structure of the region where the [O I]  $63.2 \mu\text{m}$  line is emitted. This line is predicted to arise in the disk atmosphere in the radial region between a few 10 AU and 200 AU (Woitke et al. 2009; Aresu et al. 2012). The emission region is directly exposed to the stellar radiation and models suggest that FUV and X-ray radiation are the main heating agents there. Polycyclic aromatic hydrocarbon (PAH) and dust photoelectric heating, as well as Coulomb heating, cause the gas temperature to be  $\sim 200\text{--}300$  K (Gorti & Hollenbach 2008; Meijerink et al. 2008, 2012).

In this work, we explore possible correlations of the [O I] emission with X-ray luminosity and FUV luminosity, and compare the Aresu et al. (2012) model predictions for the [O I]  $63 \mu\text{m}$  emission with data collected within the GAS in Protoplanetary DiskS (GASPS, P.I. Dent) open time key program, taken with the PACS instrument on board the *Herschel* Space Observatory (Dent et al. 2013).

In the following, we make the hypothesis that most of the [O I] emission is produced in the disk. Outflow sources, which have higher accretion rates on average, will then produce more FUV radiation and thus stronger FUV illumination of the disk surface and stronger line emission.

In Sect. 2 we present the collected observational data set, and in Sect. 3 we explain the main findings of the models studied in Aresu et al. (2012). In Sect. 4 we show the results of the comparison between model predictions and observations, which are discussed in Sect. 5. Conclusions and remarks about future work are summarized in Sect. 6.

## 2. Observations

In Table 1 we list the sources studied in this paper, together with the observed [O I] fluxes, and the collected X-ray and FUV luminosities with references. The Taurus star-forming region contains a rich population of pre-main sequence stars, with an age between 1–3 Myr. The sources in this sample have spectral types G, K, or M, and the majority of these are Class II objects. Below we describe the origin of each observed quantity listed in Table 2.

### 2.1. Oxygen line fluxes

The data reduction is described in Howard et al. (2013). The [O I]  $63 \mu\text{m}$  line was detected in 39 out of 48 class II objects observed in Taurus, and upper limits could be measured for nine more sources. Following Howard et al. (2013) we define jet/outflow sources as those objects that have a jet imaged in H $\alpha$ , [O I]  $\lambda 6300 \text{ \AA}$ , and [S II]  $\lambda 6371 \text{ \AA}$  or are associated with Herbig-Haro objects, and which show a high velocity molecular outflow or a broad ( $>50 \text{ km s}^{-1}$ ), typically blue-shifted, emission line profile in [O I]  $\lambda 6300 \text{ \AA}$  (see, e.g., Hartigan et al. 1995). These objects are labelled with a Y in Table 1. Podio et al. (2012) showed that for four of these sources (T Tau, DG Tau A, FS Tau and RW Aur) the oxygen emission at  $63 \mu\text{m}$  is spatially extended. They compared shock and disk model predictions for the fluxes of the [O I]  $63 \mu\text{m}$  line, and found that these are likely

dominated by jet/outflow emission. Following these arguments, in order to compare the data to our disk models, we only analyze [O I] fluxes from those sources in which no outflow emission has been detected (29 sources). From this sample we could retrieve the X-ray luminosity for 22 sources and the FUV luminosity for 17 sources. Both  $L_X$  and  $L_{\text{FUV}}$  were retrieved for 9 sources (Table 2).

### 2.2. X-ray luminosities

We collected the X-ray luminosity for 22 sources from the observations carried out with the *XMM-Newton* spacecraft toward the Taurus star-forming region, performed in the context of the XEST survey (P.I. Güdel). The X-ray luminosities range between  $10^{29}$  and  $10^{31}$  erg/s, which are values and associated errors taken from Güdel et al. (2007) for all the sources, except DM Tau, GM Aur, and HN Tau. For these objects,  $L_X$  was taken from Güdel et al. (2010). In the last case, as suggested by the authors, an error of  $\pm\sqrt{2}L_X$  is associated with the X-ray luminosity value to account for intrinsic variability, which is the dominant source of error.

### 2.3. FUV luminosities

We could retrieve FUV luminosities for 13 sources from Yang et al. (2012) (Table 1), the associated errors for these values are  $\sim 30\%$ . The observations were performed with the ACS camera and STIS spectrograph on board the *Hubble* Space Telescope (HST). The FUV luminosity is obtained by integrating in the  $1240\text{--}1770 \text{ \AA}$  range (7–10 eV) over the dominant line emission of C IV  $1459 \text{ \AA}$  and Si IV  $1394 \text{ \AA}$ , after continuum subtraction and correction for interstellar extinction using the law by Cardelli et al. (1989) ( $R_V = 3.1$ ). The uncertainty in the  $A_V$  and extinction law can contribute significantly to the error in the observed line fluxes. The authors assume an error in  $A_V$  of  $\sim 0.5$  mag when no errors are available. The FUV luminosity is correlated with the accretion luminosity  $L_{\text{acc}}$ . To extend the number of  $L_{\text{FUV}}$  measurements, we attempted to derive FUV luminosities for those objects in our sample that are not listed in Yang et al. (2012), using the correlations they provide for  $L_{\text{acc}}$  and  $L_{\text{FUV}}$  (in units of solar luminosity):

$$\log(L_{\text{FUV}}) = -1.67 + 0.84 \log(L_{\text{acc}}). \quad (1)$$

The FUV luminosity obtained with this prescription accounts for chromospheric and accretion-related emission. To test this method, we used  $L_{\text{acc}}$  taken from Gullbring et al. (1998) and Ingleby et al. (2009) and compared the FUV luminosity found using Eq. (1), to the one provided by Yang et al. (2012) for the sources in common.

Gullbring et al. (1998) measured the accretion luminosity as follows. The excess flux in the energy range 2.4–3.9 eV ( $3200\text{--}5100 \text{ \AA}$ ) is estimated by computing the relative veiling in the 2.8–3 eV ( $4100\text{--}4400 \text{ \AA}$ ) and 2.6–3.9 eV ( $3200\text{--}4800 \text{ \AA}$ ) bands, where clearly veiled absorption lines are available. The spectra are then corrected for the extinction. The accretion luminosity outside the 2.4–3.9 eV band is estimated by considering a slab of constant temperature and density to model the accretion spots on the stellar surface. The statistical equilibrium is solved for hydrogen, and an escape probability method is applied to estimate the emitted flux. Gullbring et al. (1998) find that the total excess flux, which is converted to accretion luminosity once the distance is known, is  $\sim 3.5$  times higher than the flux excess in

**Table 1.** Sources analyzed in this work and their properties: class, [O I] flux,  $L_X$  and  $L_{FUV}$ , and presence of an optical jet/outflow.

Name	Class	[O I] 63 $\mu\text{m}$ [1e-17 W/m <sup>2</sup> ]	[O I] 63 $\mu\text{m}$ disk only	$L_{FUV}$ [1e30 erg/s]	$L_X$ [1e30 erg/s]	Outflow [YES/NO]
AATau	II	2.2 ± 0.2	0.60	28.82 <sup>1</sup>	1.24 <sup>1.36</sup> <sub>1.11</sub>	Y
BPTau	II	0.10 ± 0.03		58.64 <sup>1</sup>	1.36 <sup>1.40</sup> <sub>1.35</sub>	N
CITau	II	3.3 ± 0.5		13.32 <sup>1</sup>	0.19 <sup>0.89</sup> <sub>0.16</sub>	N
CWTau	II	7.2 ± 0.4	0.82	111.13 <sup>2</sup>	2.84 <sup>4.00</sup> <sub>0.28</sub>	Y
CXTau	T	0.7 ± 0.3		0.68 <sup>1</sup>	–	N
CYTau	II	1.2 ± 0.4		13.32 <sup>1</sup>	0.13 <sup>0.29</sup> <sub>0.13</sub>	N
DETau	II	0.7 ± 0.6		30.41 <sup>1</sup>	–	N
DFTau	II	6.1 ± 0.6		9.95 <sup>1</sup>	–	Y
DGTau	II	134.00 ± 17.0	4.70	318.04 <sup>2</sup>	0.55 <sup>0.78</sup> <sub>0.39</sub>	Y
DHTau	II	<1.35		–	8.46 <sup>8.64</sup> <sub>8.23</sub>	N
DKTau	II	1.6 ± 0.3		18.58 <sup>2</sup>	0.92 <sup>0.96</sup> <sub>0.87</sub>	N
DLTau	II	2.2 ± 0.2		13.97 <sup>1</sup>	–	Y
DMTau	T	0.7 ± 0.2		58.28 <sup>1</sup>	2.00 <sup>2.83</sup> <sub>1.41</sub>	N
DNTau	T	0.6 ± 0.2		6.52 <sup>1</sup>	1.15 <sup>1.17</sup> <sub>1.14</sub>	N
DOTau	II	7.1 ± 1.0	1.45	470.60 <sup>1</sup>	0.24 <sup>0.34</sup> <sub>0.17</sub>	Y
DPTau	II	14.8 ± 1.3	0.57	96.29 <sup>1</sup>	0.10 <sup>0.18</sup> <sub>0.04</sub>	Y
DQTau	II	2.1 ± 0.4		0.82 <sup>2</sup>	–	N
DSTau	II	0.9 ± 0.2		49.96 <sup>1</sup>	–	N
FFTau	III	<1.01		–	0.80 <sup>1.12</sup> <sub>0.69</sub>	N
FMTau	II	1.0 ± 0.2		4.89 <sup>1</sup>	0.53 <sup>0.56</sup> <sub>0.51</sub>	N
FOTau	T	1.20 ± 0.5		–	0.06 <sup>0.52</sup> <sub>0.05</sub>	N
FQTau	II	<0.92		–	0.12 <sup>0.83</sup> <sub>0.05</sub>	N
FSTau-A	II-FS	35.8 ± 0.5		–	3.22 <sup>3.36</sup> <sub>3.09</sub>	Y
FXTau	II	<1.38		–	0.50 <sup>2.36</sup> <sub>0.39</sub>	N
GGTau	II	5.1 ± 0.4		10.51 <sup>2</sup>	–	N
GHTau	II	<0.85		–	0.11 <sup>0.12</sup> <sub>0.10</sub>	N
GI-KTau	II	3.1 ± 1.4		10.86 <sup>1</sup>	0.83 <sup>1.06</sup> <sub>0.73</sub>	N
GMAur	T	2.4 ± 0.5		28.24 <sup>1</sup>	1.60 <sup>2.26</sup> <sub>1.13</sub>	N
GOTau	II	<5.38		–	0.25 <sup>0.36</sup> <sub>0.22</sub>	N
HBC358	III	<1.4		–	0.38 <sup>0.44</sup> <sub>0.37</sub>	N
HKTau	II	3.4 ± 0.2		–	0.08 <sup>0.12</sup> <sub>0.06</sub>	N
HLTau	I	51.3 ± 0.5		–	3.84 <sup>4.73</sup> <sub>3.22</sub>	Y
HNTau	II	4.1 ± 0.2	0.56	21.29 <sup>1</sup>	0.32 <sup>0.45</sup> <sub>0.23</sub>	Y
HOTau	II	<1.03		–	0.05 <sup>0.05</sup> <sub>0.04</sub>	N
Haro6-13	II	7.0 ± 0.5		–	0.80 <sup>0.91</sup> <sub>0.14</sub>	Y
IPTau	T	0.6 ± 0.2		4.05 <sup>1</sup>	–	N
IQTau	II	1.5 ± 0.3		–	0.42 <sup>1.17</sup> <sub>0.33</sub>	N
IRAS043	II	4.9 ± 0.2		–	0.40 <sup>0.50</sup> <sub>0.37</sub>	Y
LkCa15	T	1.0 ± 0.2		4.45 <sup>3</sup>	–	N
RWAur	II	15.4 ± 0.5		–	1.60 <sup>2.26</sup> <sub>1.13</sub>	Y
RYTau	T?	10.5 ± 0.5	3.80	1042.56 <sup>1</sup>	5.52 <sup>6.38</sup> <sub>4.82</sub>	Y
SUAur	II	8.6 ± 0.3	2.51	127.42 <sup>1</sup>	9.46 <sup>9.70</sup> <sub>8.42</sub>	Y
UYAur	II	31.4 ± 0.4	2.16	27.73 <sup>2</sup>	0.40 <sup>0.57</sup> <sub>0.28</sub>	Y
UZTau	II	4.5 ± 1.4		–	0.89 <sup>1.35</sup> <sub>0.51</sub>	Y
V710Tau	II	1.0 ± 0.6		–	1.38 <sup>1.49</sup> <sub>1.32</sub>	N
V773Tau	II	6.5 ± 0.3		–	9.49 <sup>9.54</sup> <sub>9.39</sub>	Y
V819Tau	II	<0.898		–	2.44 <sup>2.61</sup> <sub>2.33</sub>	N
XZTau	II	36.1 ± 0.09		–	0.96 <sup>1.12</sup> <sub>0.86</sub>	Y

**Notes.**  $L_X$  is measured between 0.3 and 10 keV,  $L_{FUV}$  is measured between 7 and 10 eV. The oxygen fluxes listed in the fourth column are the estimated disk contribution to the total [O I] flux as explained in Sect. 5.2. The class of the objects is taken from [Andrews & Williams \(2005\)](#), X-ray luminosities between 0.3 and 10 keV are taken from [Güdel et al. \(2007, 2010\)](#), FUV luminosities with superscript 1 are retrieved from [Yang et al. \(2012\)](#) (errors are estimated to be ±30%), while the ones with superscript 2 and 3 are calculated using the accretion luminosity retrieved from [Gullbring et al. \(1998\)](#), and [Ingleby et al. \(2009\)](#) respectively (in this case the error is the one associated with the correlation: 0.38 dex). These values are then scaled by a factor 4.25 to estimate the luminosity in the 6–13.6 eV range. Outflow sources are objects for which extended emission in the optical, associated to a jet, has been observed. The [O I] emission from these objects has not been included in the primary analysis performed in this work.

**Table 2.** Taurus sources from GASPS.  $L_X$  is measured between 0.3 and 10 keV,  $L_{FUV}$  is measured between 7 and 10 eV.

Sample	[O I] detections	Upper limits	No outflow	$L_X$	$L_{FUV}$	$L_X$ and $L_{FUV}$
48	39	9	29	22	17	9

**Notes.** The last three columns only refer to sources where no outflow emission was detected.

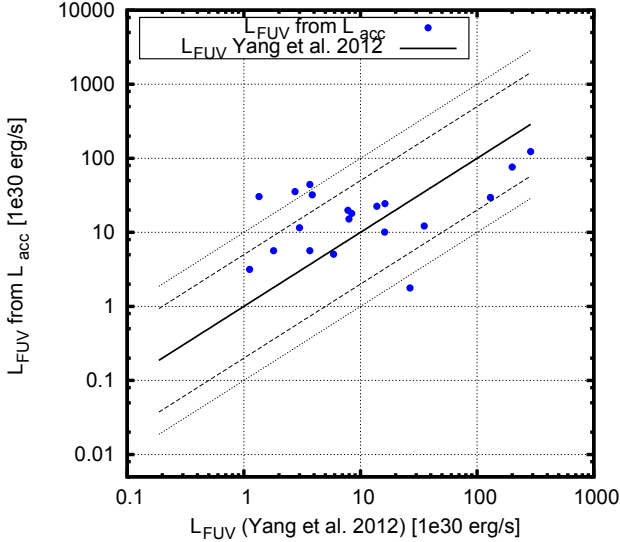


**Fig. 1.** Comparison of the  $L_{FUV}$  luminosities obtained from  $L_{acc}$  with the FUV luminosity listed in Yang et al. (2012). The solid line indicates a one-to-one ratio; dashed and dotted lines enclose the region where the new  $L_{FUV}$  are a factor 5 and 10 higher/lower than  $L_{FUV}$  obtained by Yang et al. (2012) with HST, respectively.

the 2.4–3.9 eV band. They also note that the accretion luminosity is proportional to the luminosity in the dereddened  $U$ -band, and provide fit parameters for this relation. This is used by Ingleby et al. (2009) to compute accretion luminosities for several other sources. The FUV emission in young stars is related to accretion, which is expected to be variable in time ( $\sim 0.5$  dex in days/months, Nguyen et al. 2009). Calculating the accretion luminosity by considering a collection of photometry and spectral points or from the correlation with the  $U$  broad band emission, very likely guarantees a good estimate of the overall flux in the FUV band, causing variability to average out.

We were able to obtain  $L_{FUV}$  for four sources for which [O I] has been detected, extending the sample from 13 to 17. The error associated to the derived  $L_{FUV}$  is dominated by the mean scatter in the correlation with  $L_{acc}$  (0.38 dex). It is important to note that our models define the FUV luminosity in the range between 6 and 13.6 eV (92–250 nm), while Yang et al. (2012) provides integrated fluxes from 7 to  $\sim 10$  eV (125–170 nm). We used a TW Hya spectrum composed of a collection of FUSE<sup>1</sup> (900–1190 Å) and IUE<sup>2</sup> (1150–1980 Å) data to calculate the luminosity ratio between the 6–13.6 eV and the 7–10 eV bands. The spectrum, shown in Fig. 2, was obtained by first defining resolution-dependent wavelength bins and then co-adding each dataset using the inverse square of the bin uncertainty as the summation weight. We found a conversion factor of 4.25 for TW Hya:

$$L_{FUV}^{(6-13.6 \text{ eV})} = 4.25 L_{FUV}^{(7-10 \text{ eV})}. \quad (2)$$

<sup>1</sup> <http://archive.stsci.edu/fuse/> (6 data files)

<sup>2</sup> <http://sdc.cab.inta-csic.es/cgi-ines/> (16 data files)

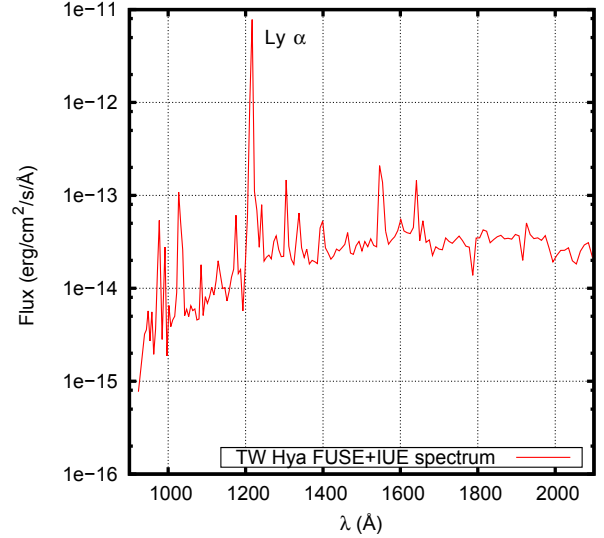


**Fig. 2.** TW Hya spectrum obtained co-adding IUE and FUSE data. This spectra is used to estimate the conversion factor between the flux in the 7–10 eV band and 6–13.6 eV band.

We applied this conversion factor to all the other objects, and from now on we refer to  $L_{FUV}$  as the FUV luminosity between 6 and 13.6 eV. A very important contribution in the FUV band is given by the  $Ly\alpha$  line emission, which can carry up to 70–90% of the total FUV flux (Schindhelm et al. 2012). However, due to resonant scattering of neutral hydrogen and deuterium in the interstellar medium (ISM), the calculation of the  $Ly\alpha$  fluxes must rely on line profile reconstruction (France et al. 2013), which is beyond the scope of this work. Moreover, Bethell & Bergin (2011) show that  $Ly\alpha$  is efficiently scattered through the atomic layers of protoplanetary disks by neutral hydrogen and dominates the energy budget over FUV continuum deeper in the disk, where the chemical environment is rich in molecules. In our models we find that the [O I] line is produced slightly above the  $H/H_2$  transition but also that the emission is insensitive to the chemical conditions. It is only sensitive to the temperature there, which is set by the interaction of the FUV continuum with PAHs and neutral carbon.

### 3. Models

In this work we use the results obtained in Aresu et al. (2012), where we used the thermo-chemical code ProDiMo (Woitke et al. 2009; Aresu et al. 2011) to calculate the [O I] 63  $\mu\text{m}$  line fluxes for a grid of 240 models. The varying parameters in the grid are  $L_X$  ( $0, 10^{29}, 10^{30}, 10^{31},$  and  $10^{32}$  erg/s),  $L_{FUV}$  ( $10^{29}, 10^{30}, 10^{31},$  and  $10^{32}$  erg/s), minimum dust grain size  $a_{min}$  (0.1, 0.3, and 1  $\mu\text{m}$ ), dust size distribution power law index  $a_{pow}$  (2.5, 3.5), and surface density distribution power law index  $\epsilon$  (1.0, 1.5). The PAH abundance is 1% with respect to the ISM abundance ( $\epsilon_{ISM} = 3 \times 10^{-7}$ ) and the dust-to-gas ratio is kept fixed at 0.01 throughout the whole disk. Following Woitke et al. (2009) we

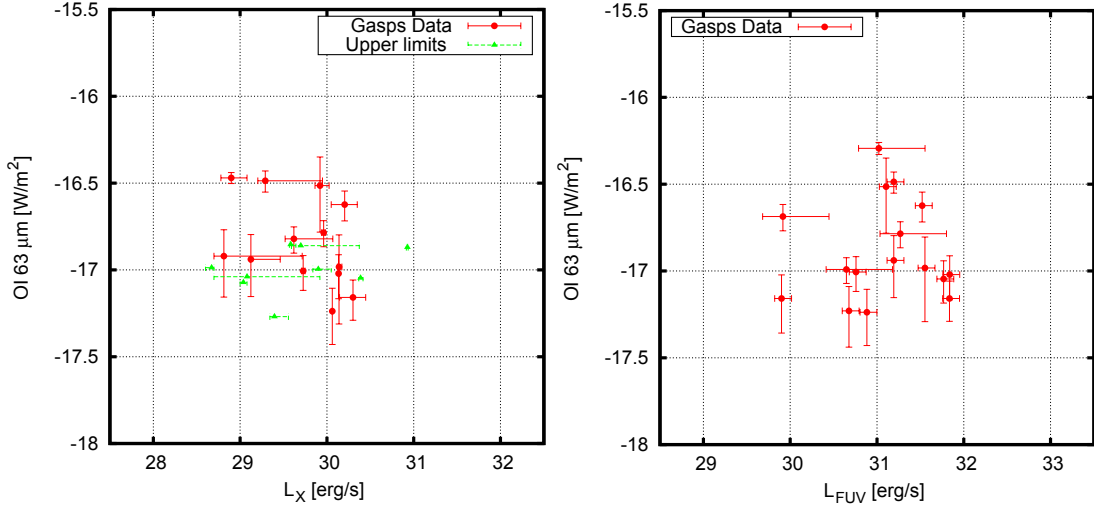


**Fig. 3.** *Left-hand panel:* flux of the [O I] 63  $\mu\text{m}$  emission versus the X-ray luminosity. *Right-hand panel:* flux of the [O I] 63  $\mu\text{m}$  emission versus the FUV luminosity. Red dots identify [O I] fluxes emitted from non-outflow sources, green diamonds are upper limits.

considered a turbulent Doppler value of  $0.15 \text{ km s}^{-1}$  (Guilloteau & Dutrey 1998; Simon et al. 2000).

As described in Aresu et al. (2012), among the parameters described above, the main effect on [O I] is caused by  $L_X$  and  $L_{\text{FUV}}$ . We then calculate the mean [O I] flux over each series of models with a given value of  $L_X$  and  $L_{\text{FUV}}$ . One series is composed of 12 models, which differ for values of  $a_{\text{min}}$ ,  $a_{\text{pow}}$  and  $\epsilon$ . The error bars accompanying the mean flux take into account a deviation of  $2\sigma$  in that sub-series of 12 models. We find that the behavior of the line flux predicted from the models (also shown in Fig. 4) is not affected by the disk inclination.

We found that the [O I] line is optically thick ( $\tau_{\text{line}} > 10^4$ ), hence sensitive to the gas temperature in the disk regions between  $r \sim 10$  and 100 AU with relative height  $z/r$  increasing from 0.2 to 0.6 (see Fig. 2 in Aresu et al. 2012). The main FUV related heating processes are photoelectric heating on PAHs, dust grains and carbon ionization heating. In all cases, these processes release a few eV into the gas phase which are converted into kinetic energy of the gas. X-ray heating proceeds via Coulomb heating, which releases larger amounts of energy due to the fast electrons released in the X-ray ionization process. We found that depending on  $L_{\text{FUV}}$  and  $L_X$  luminosities the temperature in the [O I] heating region, and consequently the line flux, is controlled by FUV or X-ray radiation or both.

In our grid of models we consider a single star, of spectral type G (see Meijerink et al. 2012, Table 1). The spread in spectral types in Taurus is restricted to objects of spectral type G, K, and M, for which the effective temperatures and bolometric luminosities agree reasonably well with our Sun-like model. This might influence the SED properties of such systems, but it does not play a role in the gas physics and chemistry in the upper layers, since this is regulated by high energy radiation.

## 4. Results

We describe the results of the observations of oxygen emission in Taurus, and investigate the correlation between the oxygen fine-structure line at 63  $\mu\text{m}$  and  $L_X$ ,  $L_{\text{FUV}}$ , and their sum. We then compare the data results to the model predictions described in Aresu et al. (2012), to study the thermal properties of the region where [O I] is emitted.

**Table 3.** Probability that a correlation is not present, estimated using Spearman and Kendall coefficients for the correlation between [O I] and  $L_X$ ,  $L_{\text{FUV}}$ , and  $L_{\text{SUM}}$  (in brackets, the probabilities for a random population in the same  $x$  and  $y$  range).

Observable	Kendall	Spearman
$L_X$	0.77 (0.60)	0.80 (0.51)
$L_{\text{FUV}}$	0.84 (0.41)	0.81 (0.40)
$L_{\text{SUM}}$	0.83	0.83

### 4.1. Observed data

In the left-hand panel of Fig. 3, we plot the [O I] fluxes versus the X-ray luminosity. The X-ray luminosity range spans  $\sim 1.5$  dex, as well as the range in [O I] fluxes. Due to the presence of upper limits, we performed survival analysis using the ASURV package (Feigelson & Nelson 1985; Isobe et al. 1986) to quantitatively investigate the presence of a correlation. In Table 3, we summarize the results obtained showing the probability that the correlation is not present using a Spearman and Kendall statistical test. This has been done for the data sample and for a random population of values in the same ranges (in brackets).

In the right-hand panel of Fig. 3, we plot the [O I] fluxes versus  $L_{\text{FUV}}$ . Also in this case there is no clear correlation between [O I] and the FUV luminosity. We found similar results concerning the correlation between [O I] and  $L_{\text{SUM}} = L_X + L_{\text{FUV}}$  (Table 3).

### 4.2. Modeling

In the left-hand panel of Fig. 4 we show the results taken from the grid of models described in Meijerink et al. (2012) and Aresu et al. (2012), each colored stripe is a series of [O I] fluxes for models with a given FUV luminosity. The thickness of the stripe accounts for all the models with different dust parameters and disk surface density distributions (see Aresu et al. 2012 for the details). The models agree quantitatively with the data, reproducing the same [O I] flux range from low to high FUV luminosity along the 2 dex interval in  $L_X$ . The models do not predict a correlation between [O I] and  $L_X$ , but rather a threshold

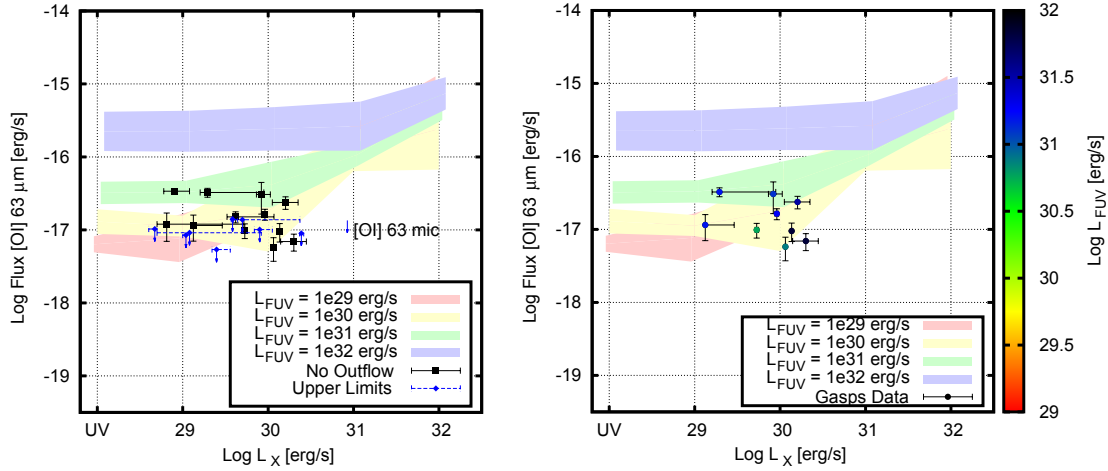


**Fig. 4.** Models and observations. FUV luminosity ranges from  $10^{29}$  (red stripe) to  $10^{32}$  erg/s (blue stripe). When stripes overlap, the stripe representing a higher luminosity is shown. In the *right-hand panel* the data points are color-coded for the FUV luminosity of a given object, following the color scale presented in the side bar.

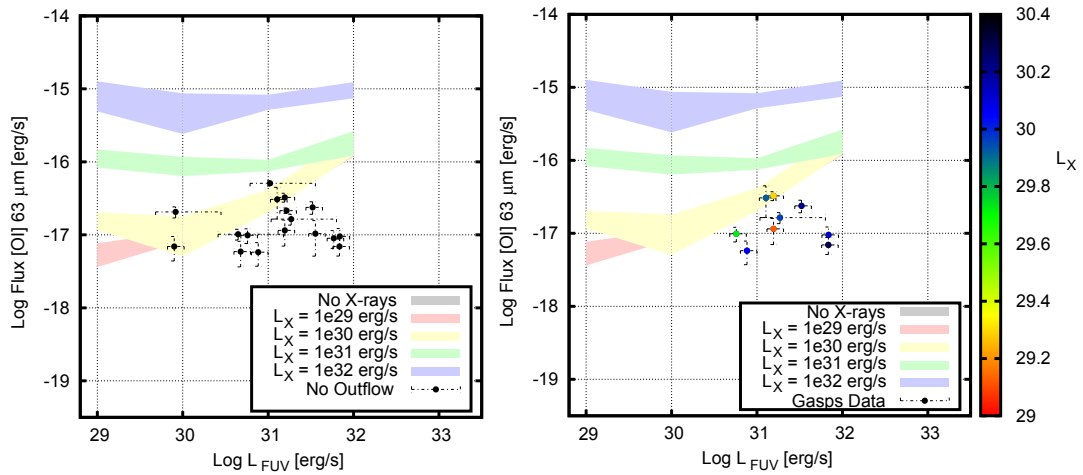


**Fig. 5.** Flux of the [O I]  $63 \mu\text{m}$  line versus  $L_{\text{FUV}}$ . The colored stripes represent predicted values for different  $L_X$ .

behavior: for  $L_X > 10^{30}$  erg/s and  $L_X > L_{\text{FUV}}$ , [O I] emission should be dominated by X-rays.

The models also suggest that at a given X-ray luminosity, the [O I] line flux scales with  $L_{\text{FUV}}$ . To test this on a qualitative basis, in the right-hand panel of Fig. 4, we plot the [O I] observed line fluxes versus the X-ray luminosity, color-coding for the observed FUV luminosity. The predicted [O I] fluxes from the models seem to overestimate (factor  $\sim 5$ ) the observations at a given  $L_{\text{FUV}}$ . This can be also seen in Fig. 5, where the predicted [O I] is on average higher than the data. In this plot the stripes are color-coded for different  $L_X$ . These findings depend strongly on how the FUV luminosity is scaled from the 7–10 eV band to the 6–13.6 band. We use the same stellar template (TW Hya) to estimate the variation in the flux in the full FUV range. However this might not be applicable to each object. Moreover, we do not consider the  $\text{Ly}\alpha$  flux in our models, which might cause an overestimate of the continuum flux in the FUV band, which could cause extra FUV heating in the [O I] emission region, hence overestimating its line flux.

Figure 2 in Aresu et al. (2012, right-hand panel) shows that the energy deposition rates associated with  $L_X$  and  $L_{\text{FUV}}$  are comparable. We therefore explored a correlation between [O I] and the simple sum of these luminosities. We fit the data using a linear function. Figure 6 shows the data and the fit to the model

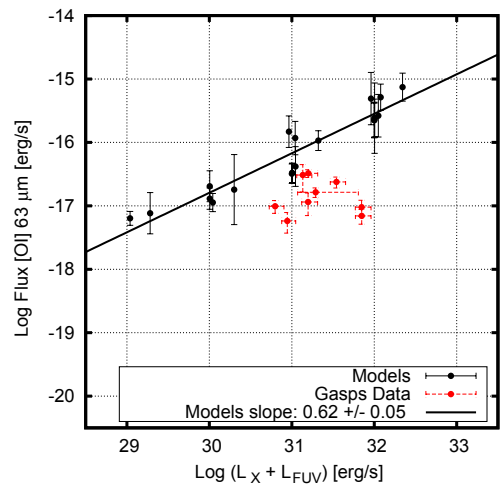


**Fig. 6.** [O I] flux versus  $L_X + L_{\text{FUV}}$ . Model points are black, while data points are red. In our models we considered a sun-like star surrounded by a disk of  $0.02 M_\odot$  which extends from 0.5 to 500 AU.

points. Given that all the sources in the observed sample have  $L_X$  between  $10^{29}$  and  $10^{31}$  erg/s, we did not include the [O I] flux for those models that have  $L_X = 0$  or  $10^{32}$  erg/s, obtaining a slope of 0.6.

## 5. Discussion

We discuss here the results presented in the previous section, analyzing the capability of the models in interpreting the data and suggest improvements to be made.

### 5.1. FUV luminosity

Our  $L_{\text{FUV}}$  estimates rely on calculating the scale factor that we adopted to get the luminosity in the 6–13.6 band (needed to compare the data to our models) out of the 7–10 eV band used by Yang et al. (2012). These values can be further improved for two reasons: (1) we calculated the conversion factor for TW Hya alone, and used it for the whole sample; (2) the Ly- $\alpha$  profile in the TW Hya spectrum should be reconstructed to account for neutral hydrogen absorption in the ISM. Nevertheless, the slope in Fig. 6 weakly depends on this reconstruction. A change of a factor 2 in the conversion factor would cause a  $\sim 20\%$  change in the slope.

### 5.2. Possible correlations

Assuming that the measured [O I] fluxes are mainly emitted from the disk, we find that both the models and the data suggest that there is no correlation between [O I] 63  $\mu\text{m}$  and  $L_X$  or  $L_{\text{FUV}}$  in the range of luminosities spanned by our sample. According to our models this is caused by the FUV-related heating processes affecting the line at a given X-ray luminosity, causing a vertical scatter ( $\sim 2$  dex) comparable to the range of X-ray luminosities observed in T Tauri stars. The same conclusions can be drawn when [O I] is plotted against  $L_{\text{FUV}}$ , where the vertical scatter is now to ascribe to Coulomb heating.

This amount of scatter is partially seen in the data ( $\sim 1$  dex), and no correlation between [O I] and  $L_{\text{FUV}}$  emerges. All the sources investigated here have  $L_{\text{FUV}} > L_X$ , and 90% of them have  $L_{\text{FUV}} > 10 \times L_X$ . Disk models would predict higher [O I] emission (factor  $\sim 10$ ) for  $L_{\text{FUV}} > 10^{31}$  erg/s, but the data shows that higher [O I] fluxes are achieved only when outflows are present.

With the aim of extending our data sample, we also included outflow sources and proceeded to estimate the [O I] disk emission as follows. Howard et al. (2013) find a correlation between [O I] and the continuum at 63  $\mu\text{m}$  for non-outflow sources. Outflow sources stand clearly above this correlation (see their Fig. 6). Using the fit formula that they provided, we estimated the disk emission for outflow sources by subtracting the amount of excess flux with respect to the fit from the total [O I] emission (Table 1, fourth column). In this way we enlarge our sample (though only through estimated disk emission) and attempt to check for the absence of a clear correlation with  $L_{\text{FUV}}$  and  $L_X$ . In fact, even for the enhanced sample, we find no correlation with either one of these quantities or with their sum.

### 5.3. Heating mechanism

Since the PACS data is spatially and spectrally unresolved, the location of the [O I] 63  $\mu\text{m}$  emission is unclear. If most of the emission for non-outflow sources originates in the disk, both  $L_X$  and  $L_{\text{FUV}}$  are important heating agents in the [O I] emitting region, but their direct influence on the [O I] emission remains elusive. In Aresu et al. (2012), we suggested a threshold mechanism for [O I] with respect to  $L_X$ . This cannot be tested with our current data set, as there are no sources that have  $L_X$  higher than a few times  $10^{30}$  erg/s.

### 5.4. Impact of other parameters

*Spitzer* observations toward 38 T Tauri stars performed by Geers et al. (2006), detected PAH features in only 8% of the objects. Models of PAH chemistry in disks surrounding T Tauri stars suggest that these species do exist, but the UV luminosity of the central star is just too weak to reveal their presence. PAH emission is indeed believed to be a factor 10 weaker in T Tauri stars than in Herbig Ae/Be stars, where the UV luminosity is orders of magnitude higher. The authors also suggest that the PAH abundance in T Tauri stars is a factor 10 or 100 lower than the one inferred for the ISM.

In our grid we used a PAH abundance 0.012 times lower than the PAH abundance in the ISM. Nevertheless, we found PAH heating to be the main FUV-driven heating process in the [O I] emission region. The second most efficient heating processes are  $\text{C}^+$  heating and photoelectric heating on dust grains. The sum of these heating processes is less than a factor two lower than PAH heating, and it follows the same behavior with respect to  $L_{\text{FUV}}$ . An even lower PAH abundance would just cause a lower temperature in the [O I] emission region, thus weakening the line emission, but not affecting the nature of the correlation we predict.

On the other hand, we considered in our models only a limited set of free parameters ( $L_X$ ,  $L_{\text{FUV}}$ , minimum dust size, dust size distribution power law, and the surface-density distribution power law). However, the [O I] flux can be affected by other quantities, such as the flaring index  $\beta$ , dust settling, gas-to-dust mass ratio, and outer radius (Woitke et al. 2010; Kamp et al. 2011). In the disk models used in this work, the flaring angle is a result of the hydrostatic equilibrium (Meijerink et al. 2012), and the solutions we find for the scale height generally point toward maximum flared disks ( $\beta \sim 1.25$ ). This may not be representative of the disks in our sample especially when dust settling takes place, leading to flatter geometries, for which  $\beta \leq 1$  (Dullemond & Dominik 2005). Flat disks absorb less radiation, thereby diminishing the importance its importance, hence its impact on the gas emission.

Dust settling should also affect the dust-to-gas mass ratio, which is usually kept fixed to the ISM value ( $\delta = 0.01$ ) at each point in the disk. Variations in the latter would change the opacity throughout the disk causing different properties in the energy deposition distribution of the FUV radiation.

In our models we keep the disk's outer radius fixed at 500 AU to allow proper comparison with previous works. However disks surrounding T Tauri stars do range in size from 50 AU to hundreds of AU (Williams & Cieza 2011); for example because of the reduced emitting area, smaller disks illuminated by high FUV luminosities do not necessarily yield higher [O I] fluxes when compared to bigger disks illuminated by lower  $L_{\text{FUV}}$ .

The disk mass also affects the [O I] emission. In Taurus the spread in disk masses is estimated to be  $\sim 2$  dex:  $M_D/M_\odot \sim 10^{-1.5} - 10^{-3.5}$  (Andrews et al. 2013). This spread could cause  $\sim 1$  dex scatter in the [O I] emission (Woitke et al. 2011), hence affecting the correlations studied in this work.

## 6. Conclusions and outlook

In this work we studied the impact of FUV and X-ray radiation on the thermal balance in the oxygen emission region for protoplanetary disks surrounding T Tauri stars. We compared disk model predictions with observations of the [O I] 63  $\mu\text{m}$  line toward protoplanetary disks that do not show outflow emission in the Taurus region obtained with the PACS instrument on board

*Herschel*. The observations show no correlation between the [O I] 63  $\mu\text{m}$  line emission and the X-ray luminosity, the FUV luminosity, or their sum.

Our thermo-chemical disk models calculated with ProDiMo show that our predictions on the [O I] fluxes qualitatively agree with the observations. There is no correlation between [O I] and  $L_X$  or  $L_{\text{FUV}}$ , as the data suggest. Nevertheless, the models predict a correlation between [O I] and the sum  $L_X + L_{\text{FUV}}$ , but it is not seen in the data. The reason can be the limited set of parameters varied in our model ( $L_X$ ,  $L_{\text{FUV}}$ , grain minimum size, power law of the grain size distribution, and power law of the surface density distribution) grid to understand the relative importance of  $L_X$  and  $L_{\text{FUV}}$ .

However, other parameters can affect the [O I] line, causing the correlation we predict to vanish when a more complete grid is used.

To include all the disk parameters that influence the [O I] line, a different set of models should be used. Flatter disk geometries should be included, as well as a proper treatment of X-ray and FUV physics and dust settling (local variations in the gas-to-dust mass ratio).

Moreover, these models should be compared to a higher number of observations: high spatial and spectral resolution data is required to disentangle the location of the emission region of the line. In many sources that drive outflows, the contribution of the disk to the total flux of the line remains unclear.

More measurements of  $L_{\text{FUV}}$  would also be necessary. To test the threshold mechanisms proposed in our previous work, observations of [O I] of sources with  $L_X > L_{\text{FUV}}$ , if any, are essential.

The understanding of the [O I] dependence on the FUV and X-ray radiation makes it possible to investigate the gas surface layers above the H/H<sub>2</sub> transition. Such studies are very interesting for understanding the photoevaporation mechanism and how it may drive disk evolution across the transition from one optically thick to a debris disk.

*Acknowledgements.* We thank Aki Roberge for her comments on the FUV analysis, which helped to improve the paper, and Glenn White for thoroughly reading the paper. W.F.T., P.W., F.M., M.G., and I.K. acknowledge funding from the EU FP7-2011 under Grant Agreement Nr. 284405. L.P. acknowledges funding from the FP7 Intra-European Marie Curie Fellowship (PIEF-GA-2009-253896).

## References

- Alexander, R. D., Clarke, C. J., & Pringle, J. E. 2006, *MNRAS*, 369, 216  
 Andrews, S. M., & Williams, J. P. 2005, *ApJ*, 631, 1134  
 Andrews, S. M., Rosenfeld, K. A., Kraus, A. L., & Wilner, D. J. 2013, *ApJ*, 771, 129  
 Aresu, G., Kamp, I., Meijerink, R., et al. 2011, *A&A*, 526, A163  
 Aresu, G., Meijerink, R., Kamp, I., et al. 2012, *A&A*, 547, A69  
 Bethell, T. J., & Bergin, E. A. 2011, *ApJ*, 739, 78  
 Calvet, N., & Gullbring, E. 1998, *ApJ*, 509, 802  
 Cardelli, J. A., Clayton, G. C., & Mathis, J. S. 1989, *ApJ*, 345, 245  
 Dent, W. R. F., Thi, W. F., Kamp, I., et al. 2013, *PASP*, 125, 477  
 Dullemond, C. P., & Dominik, C. 2005, *A&A*, 434, 971  
 Ercolano, B., Drake, J. J., Raymond, J. C., & Clarke, C. C. 2008, *ApJ*, 688, 398  
 Feigelson, E. D., & Nelson, P. I. 1985, *ApJ*, 293, 192  
 France, K., Froning, C. S., Linsky, J. L., et al. 2013, *ApJ*, 763, 149  
 Geers, V. C., Augereau, J.-C., Pontoppidan, K. M., et al. 2006, *A&A*, 459, 545  
 Glassgold, A. E., Najita, J., & Igea, J. 2004, *ApJ*, 615, 972  
 Glassgold, A. E., Najita, J. R., & Igea, J. 2007, *ApJ*, 656, 515  
 Gorti, U., & Hollenbach, D. 2008, *ApJ*, 683, 287  
 Gorti, U., Dullemond, C. P., & Hollenbach, D. 2009, *ApJ*, 705, 1237  
 Güdel, M., Briggs, K. R., Arzner, K., et al. 2007, *A&A*, 468, 353  
 Güdel, M., Lahuis, F., Briggs, K. R., et al. 2010, *A&A*, 519, A113  
 Guilloteau, S., & Dutrey, A. 1998, *A&A*, 339, 467  
 Gullbring, E., Hartmann, L., Briceno, C., & Calvet, N. 1998, *ApJ*, 492, 323  
 Hartigan, P., Edwards, S., & Ghandour, L. 1995, *ApJ*, 452, 736  
 Howard, C. D., Sandell, G., Vacca, W. D., et al. 2013, *ApJ*, 776, 21  
 Ingleby, L., Calvet, N., Bergin, E., et al. 2009, *ApJ*, 703, L137  
 Isobe, T., Feigelson, E. D., & Nelson, P. I. 1986, *ApJ*, 306, 490  
 Jonkheid, B., Faas, F. G. A., van Zadelhoff, G.-J., & van Dishoeck, E. F. 2004, *A&A*, 428, 511  
 Kamp, I., & Dullemond, C. P. 2004, *ApJ*, 615, 991  
 Kamp, I., Woitke, P., Pinte, C., et al. 2011, *A&A*, 532, A85  
 Meijerink, R., Glassgold, A. E., & Najita, J. R. 2008, *ApJ*, 676, 518  
 Meijerink, R., Aresu, G., Kamp, I., et al. 2012, *A&A*, 547, A68  
 Nguyen, D. C., Scholz, A., van Kerkwijk, M. H., Jayawardhana, R., & Brandeker, A. 2009, *ApJ*, 694, L153  
 Nomura, H., Aikawa, Y., Tsujimoto, M., Nakagawa, Y., & Millar, T. J. 2007, *ApJ*, 661, 334  
 Podio, L., Kamp, I., Flower, D., et al. 2012, *A&A*, 545, A44  
 Schindhelm, E., France, K., Herczeg, G. J., et al. 2012, *ApJ*, 756, L23  
 Simon, M., Dutrey, A., & Guilloteau, S. 2000, *ApJ*, 545, 1034  
 Valenti, J. A., Johns-Krull, C. M., & Linsky, J. L. 2000, *ApJs*, 129, 399  
 Williams, J. P., & Cieza, L. A. 2011, *ARA&A*, 49, 67  
 Woitke, P., Kamp, I., & Thi, W. 2009, *A&A*, 501, 383  
 Woitke, P., Pinte, C., Tilling, I., et al. 2010, *MNRAS*, 405, L26  
 Woitke, P., Riaz, B., Duchêne, G., et al. 2011, *A&A*, 534, A44  
 Yang, H., Herczeg, G. J., Linsky, J. L., et al. 2012, *ApJ*, 744, 121